IOP Publishing Journal of Physics A: Mathematical and Theoretical
J. Phys. A: Math. Theor. **53** (2020) 154002 (23pp) https://doi.org/10.1088/1751-8121/ab78cc

Synchronization in complex networks with long-range interactions

Sarbendu Rakshit, Soumen Majhi and Dibakar Ghosh[1]

Physics and Applied Mathematics Unit, Indian Statistical Institute, 203 B. T. Road, Kolkata-700108, India

E-mail: dibakar@isical.ac.in

Received 31 August 2019, revised 24 January 2020
Accepted for publication 21 February 2020
Published 23 March 2020

Abstract

Variants of collective behavior can materialize in large ensembles of coupled dynamical systems, and synchronization is one of the most significant among them due to its enormous applicability from neuronal networks to finance. At the same time, current study of long-range interactions is attracting researchers' attention mainly because interactions among dynamical units in a network may not be present only in the form of short-range direct communications, but also through the long-range connections arising along the long-distant paths among the nodes. Despite a few recent works on synchronization in long-range interacting systems, there are still a lot of areas regarding the influences of long-range communications on top of non-regular complex networks that remain unexplored. Here we derive local and global asymptotic stability conditions for complete synchronization manifold with k-path Laplacian matrices. Importantly, we show that the analytical findings are in excellent agreement with the numerical results. For the numerical illustrations, we contemplate with the Erdös–Rényi random network by means of a long-range connection governed by the power-law and demonstrate the emergence of complete synchronization. We particularly examine the synergy between the coupling strength and the power-law exponent.

Keywords: synchronization, long-range interaction, master stability function, global stability

(Some figures may appear in colour only in the online journal)

[1]Author to whom any correspondence should be addressed.

1. Introduction

Oscillatory dynamical systems in nature are rarely isolated and interactions among these dynamical units often give rise to new phenomena. Reserches of past two decades on macroscopic behavior of coupled oscillators' network have enhanced our perception of various natural, man-made and social systems. Among those collective dynamical behaviors, the vibrant phenomenon of synchronization [1–3] has been in the focus of intense research in diverse area of science. At the same time, complex networks have been very competent in describing the underlying interactional framework and hence the universal properties of many complex systems. In this context, it has been demonstrated that the correlation between the network architecture and the local dynamics is really crucial as far as the emergence of synchrony is concerned.

In recent times, the process of synchronization has been studied in networks under different forms of structural complexities, e.g., in weighted networks [4, 5], time-varying networks [6, 7], multiplex networks [8, 9], and time-varying multiplex networks [10–12] etc. On the other hand, long-range interacting systems [13–19] have come up to be one of the most promising areas of research in complex systems ranging from mechanical to biological oscillatory networks [20]. To be precise, long-range interaction owing to power-law decay has been studied in biological networks [21], ferromagnetic spin models [22], hydrodynamic interaction of active particles [23, 24]. Power-law interactions arise in many other systems like nuclear spins in solid-state systems [25], Rydberg atoms [26], plasmas [27] etc. Nevertheless, except only a few notable attempts [28–36], the effect of indirect communications in the form of long-range interactions on the synchronization phenomenon has rather been ignored. Although the references [28, 30, 31] studied synchronization in a population of phase oscillators over a lattice with decaying coupling, whereas Anteneodo *et al* [29] investigated the influence of long-range interactions for coupled-map lattices. Diverse chimeric patterns including that in juxtaposition with oscillation death state are studied in the reference [32]. Enhancement in persistence of metapopulation via asynchrony due to long-range dispersal has been discussed lately [33]. Network synchronizability due to long-range interaction for Mellin and Laplace transformed is reported recently [34, 35]. Sathiyadevi *et al* [36] have come up with their results on various collective behaviors including synchronization, oscillation death and solitary states because of long-range interaction with repulsive and symmetry breaking coupling functions. But, in most of the cases either only phase oscillator models have been dealt with or the underlying network framework has been presumed to be regular networks with ring structures. Furthermore, a thorough analysis of the stability of the synchronization manifold is still missing in the literature.

Motivated by these key facts, we consider long-range interactions among the constituents (nodes in the form of chaotic dynamical systems) of a network built upon a non-regular (complex) network. In contrast to the earlier works considering completely regular networks, mostly the one-dimensional rings of nodes, we here construct a general mathematical framework for complete synchronization state using long-range interactions. Then we mathematically derive the existence condition on the network topology to derive synchronization. We investigate local stability analysis through the master stability function (MSF) approach [37] that shows excellent match with the numerically obtained results. The MSF approach serves as an effective tool for analyzing local stability of the synchronization phenomena in complex networks. Basically, it reduces the synchronization problem of the coupled systems to a fixed point problem of an uncoupled system. Lastly, we also derive the condition of global stability for complete synchronization state with the help of an appropriate Lyapunov function. This Lyapunov function

is made upon a differential framework for analyzing the convergence of the trajectories of nonlinear system toward each other. It belongs to a class of incremental stability method, leading to global results. For numerical simulations, as an exemplar, we consider paradigmatic chaotic Lorenz system as the dynamics of each node and Erdös–Rényi (ER) random network [38, 39] as the underlying network. Rigorous parameter regions are drawn for synchronization as a function of random connectivity probability p, coupling strength ϵ and power-lay exponent α. The numerical results are in excellent agreement with our analytical findings.

The rest of the paper is assembled as follows. Some basic graph theoretical and mathematical preliminaries are recalled in section 2. In section 3, we then introduce the mathematical network model in terms of the k-path adjacency or Laplacian matrices that assumes long-range connections together with direct short-range couplings. The local stability condition for synchronization state is analyzed in section 4. Numerical illustrations of our theoretical findings are discussed in section 5. Section 6 deals with the global stability of the state of synchrony and numerical explanations. Finally, we provide conclusion on our findings in section 7.

2. Graph theoretical and mathematical preliminaries

In this section, some useful graph theoretical and mathematical preliminaries are described.

Consider a graph $G = (V, E)$ with N number of vertices, i.e., $V = \{v_1, v_2, \ldots, v_N\}$, and $E \subset V \times V$ is the set of undirected edges. The length of a shortest path between v_i and v_j is called the distance between the nodes v_i and v_j, which is denoted by $d(v_i, v_j)$. Then the diameter of the graph can be defined as $d_{\max} = \max\{d(v_i, v_j) : i, j = 1, 2, \ldots, N\}$.

The k-path adjacency matrix $\mathscr{A}^{[k]}$ of the underlying network is then defined as the square symmetric $N \times N$ matrix whose entries are given by

$$\mathscr{A}_{ij}^{[k]} = \begin{cases} 1 & \text{if } d(i, j) = k, \\ 0 & \text{otherwise.} \end{cases} \tag{1}$$

This k-path adjacency matrix exists up to $k = d_{\max}$, since no path exists of length greater than the diameter $d_{\max}$. Therefore, the range of k is $k = 1, 2, \ldots, d_{\max}$.

In order to explain the definition of k-path networks, we consider a small exemplary network consisting of $N = 6$ nodes with $d_{\max} = 3$ and plot the corresponding k-path ($k = 1, 2, 3$) networks along with the associated adjacency matrices in figure 1. Figure 1(a) depicts the underlying network, more specifically the one-path network, with the adjacency matrix $\mathscr{A}^{[1]}$. In this one-path network $(v_1, v_2) \in E$ and $(v_2, v_3) \in E$, but $(v_1, v_3) \notin E$, thus $d(v_1, v_3) = 2$ and $\mathscr{A}_{13}^{[2]} = 1$. In this way, the two-path network is formed in figure 1(b). Observe that, the two-path network is also connected. Now $(v_3, v_6) \in E$, so there is a path of length three from the vertex v_1 to the vertex v_6, namely $(v_1, v_2) \to (v_2, v_3) \to (v_3, v_6)$. But in this network there is no such path from v_1 to v_6 which is of length less than three. Therefore, $d(v_1, v_6) = 3$, this yields $\mathscr{A}_{16}^{[3]} = 1$. Also there is another one path of length three, from v_6 to v_4. Hence, the three-path network comprises of only two edges (v_1, v_6) and (v_6, v_4). Remaining three vertices v_2, v_3 and v_5 are isolated in this network. The pictorial view of this network is delineated in figure 1(c), with corresponding adjacency matrix $\mathscr{A}^{[3]}$.

In general, the k-path Laplacian matrix $\mathscr{L}^{[k]}$ of the underlying network can be expressed as

$$\mathscr{L}_{ij}^{[k]} = \begin{cases} -\mathscr{A}_{ij}^{[k]} & \text{if } i \neq j, \\ \sum_{j=1}^{N} \mathscr{A}_{ij}^{[k]} & \text{if } i = j, \end{cases} \tag{2}$$

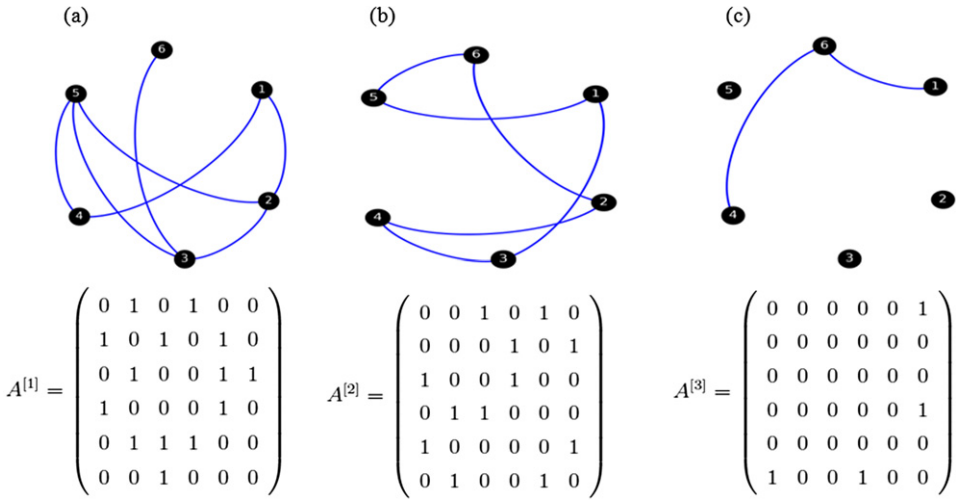

$$A^{[1]} = \begin{pmatrix} 0 & 1 & 0 & 1 & 0 & 0 \\ 1 & 0 & 1 & 0 & 1 & 0 \\ 0 & 1 & 0 & 0 & 1 & 1 \\ 1 & 0 & 0 & 0 & 1 & 0 \\ 0 & 1 & 1 & 1 & 0 & 0 \\ 0 & 0 & 1 & 0 & 0 & 0 \end{pmatrix} \quad A^{[2]} = \begin{pmatrix} 0 & 0 & 1 & 0 & 1 & 0 \\ 0 & 0 & 0 & 1 & 0 & 1 \\ 1 & 0 & 0 & 1 & 0 & 0 \\ 0 & 1 & 1 & 0 & 0 & 0 \\ 1 & 0 & 0 & 0 & 0 & 1 \\ 0 & 1 & 0 & 0 & 1 & 0 \end{pmatrix} \quad A^{[3]} = \begin{pmatrix} 0 & 0 & 0 & 0 & 0 & 1 \\ 0 & 0 & 0 & 0 & 0 & 0 \\ 0 & 0 & 0 & 0 & 0 & 0 \\ 0 & 0 & 0 & 0 & 0 & 1 \\ 0 & 0 & 0 & 0 & 0 & 0 \\ 1 & 0 & 0 & 1 & 0 & 0 \end{pmatrix}$$

Figure 1. Examples of k-path networks (upper panel) and their corresponding adjacency matrices (lower panel): (a) $k = 1$, i.e., the original network, (b) $k = 2$, i.e., the two-path network extracted from (a), and (c) $k = 3$, i.e., the three-path network extracted from (a).

for all $k = 1, 2, \ldots, d_{\max}$. These k-path Laplacians are zero-row sum matrices. Thus all of them has a zero eigenvalue. For disconnected network, the multiplicity of this eigenvalue is more than one for these matrices. If the underlying network is connected then the zero eigenvalue is simple for $\mathscr{L}^{[1]}$. But there is no certainty that it will remain simple for all $\mathscr{L}^{[k]}$, $k = 2, 3, \ldots, d_{\max}$. In our schematic diagram (cf figure 1), for connected one-path network, the two-path network is also connected. But, the three-path network does not remain connected. It has four components, so for this case, the multiplicity of the zero eigenvalue of $\mathscr{L}^{[3]}$ is four.

Let $\gamma_i^{[k]}$ $(i = 1, 2, \ldots, N)$ be the eigenvalues of $\mathscr{L}^{[k]}$ for $k = 1, 2, \ldots, d_{\max}$. Then $\mathscr{L}^{[k]}$ has at least one zero eigenvalue, say $\gamma_1^{[k]}$ corresponding to the eigenvector $\mathbb{1}_N = [1, 1, \ldots, 1]^{\text{tr}}$. If the one-path network is undirected then all the k-path Laplacians $\mathscr{L}^{[k]}$ become symmetric matrices. Thus, all of them can be orthogonally diagonalizable by their individual basis of eigenvectors. Therefore, if $V^{[k]}$ is the corresponding matrix of orthogonal eigenvectors of the real symmetric matrix $\mathscr{L}^{[k]}$, then we get $\mathscr{L}^{[k]} = V^{[k]} D^{[k]} V^{[k]^{-1}}$, where $D^{[k]} = \text{diag}\left\{\gamma_1^{[k]}, \gamma_2^{[k]}, \ldots, \gamma_N^{[k]}\right\}$.

Notations: Throughout our manuscript, $O_{p\times q}$ denotes $p \times q$ order zero matrix, I_p denotes the identity matrix of order p, while $\mathbb{1}_p$ is a column matrix with each element one. $\oplus$ denotes the matrix direct sum and $\otimes$ denotes the matrix Kronecker product. $\|\mathbf{x}\|$ denotes the Euclidean norm of $\mathbf{x}$ and defined by $\|\mathbf{x}\| = \sqrt{\sum_{i=1}^{d} |x_i|^2}$, where d is the dimension of $\mathbf{x}$.

3. The network model

Now, we assume that each node in the network is associated with a d-dimensional dynamical system. Then the nodal dynamics of the ith node in the network possessing long-range interaction can be described as follows,

$$\dot{\boldsymbol{x}}_i = f(\mathbf{x}_i) + \sum_{k=1}^{d_{\max}} \epsilon_k \sum_{j=1}^{N} \mathscr{A}_{ij}^{[k]} \Gamma(\mathbf{x}_j - \mathbf{x}_i), \tag{3}$$

where $\mathbf{x}_i$ represents the d-dimensional state variable of the ith node, $f:\mathbb{R}^d \to \mathbb{R}^d$ is a sufficiently smooth vector field describing the dynamics of each isolated node, ϵ_k is the coupling strength between the ith and jth nodes if $d(i,j)=k$, which determines how the information propagates among these two nodes depending on their shortest distance. That is, the ith and jth nodes are k-path connected, where $k=1,2,\ldots,d_{\max}$ with $d_{\max}$ is the diameter of the network. $\mathscr{A}^{[k]}$ is the k-path adjacency matrix and Γ is the inner coupling matrix determining the state variables through which the nodes are interacting with each other.

When complete synchronization occurs in the dynamical network (3), then all the nodes evolve in unison, i.e., with the identical trajectory. Then, there exists a trajectory $\mathbf{x}_0 \in \mathbb{R}^d$, such that, for each $\epsilon > 0$ (however small) there exists $T > 0$ (however large), $\|\mathbf{x}_i(t) - \mathbf{x}_0(t)\| < \epsilon$ whenever $t \geqslant T$.

Observation 1. The state variable $\mathbf{x}_0$ of the complete synchronization manifold obeys the evolution equation $\dot{\boldsymbol{x}}_0 = f(\mathbf{x}_0)$.

We call the subset $\mathcal{S} = \left\{\mathbf{x}_0 \subset \mathbb{R}^d : \mathbf{x}_i = \mathbf{x}_0, \quad \forall\, i = 1,2,\ldots,N\right\}$ as the complete synchronization manifold. Our aim of this paper is to determine the local and global stability of $\mathcal{S}$ in terms of the coupling and network parameters.

Here we note that we are considering bidirectional coupled network. So, $\mathscr{A}^{[k]}$ is a symmetric matrix and hence $\mathscr{L}^{[k]}$ is also symmetric for all k. Therefore, $\mathscr{L}^{[k]}$ $(k=1,2,\ldots,d_{\max})$ is orthogonally diagonalizable by its basis of eigenvectors.

4. Local stability analysis

At first, we will analytically determine the local stability condition of the synchronization state for the coupled system (3). For this, we adopt the seminal MSF approach [37]. Our entire theoretical analysis is associated with all the k-path Laplacians. In this purpose, we need the following assumptions.

Assumption 1. The individual nodal dynamics f is continuously differentiable with respect to its argument.

The above assumption confirms us about the Taylor series expansion of the nodal evolution function f about the synchronization trajectory with respect to small perturbations.

Theorem 2 (Linear stability analysis)**.** *The parallel and transverse components along the synchronous solution respectively satisfy the system of equations,*

$$\begin{aligned}
\dot{\eta}_{\mathrm{P}}(t) &= Jf(\mathbf{x}_0)\eta_{\mathrm{P}}(t),\\
\dot{\eta}_{\mathrm{T}_i}(t) &= \left[Jf(\mathbf{x}_0) - \epsilon_1\gamma_i{}^{[1]}\Gamma\right]\eta_{\mathrm{T}_i} - \sum_{k=2}^{d_{\max}}\epsilon_k\sum_{j=1}^{N-1}U_{ij}{}^{[k]}\Gamma\eta_{\mathrm{T}_j}, \quad i=2,3,\ldots,N. \quad (4)
\end{aligned}$$

Here, Jf denotes the Jacobian of the function f. $\eta_{\mathrm{P}}(t)\in\mathbb{R}^d$ and $\eta_{\mathrm{T}}(t)\in\mathbb{R}^{d(N-1)}$ are the state vectors which evolve parallel and transverse to the synchronization solution, respectively.

Proof of Theorem 2. In the state of complete synchronization, each individual oscillator exhibits identical time evolution for appropriate interaction among the dynamical units. Let, at the state of complete synchrony, the entire network evolves according to $\mathbf{x}_i(t) = \mathbf{x}_0(t), \forall i = 1,2,\ldots,N$. Here $\mathbf{x}_0(t)$ is the state variable corresponding to the synchronization manifold satisfying $\dot{\boldsymbol{x}}_0 = f(\mathbf{x}_0)$. Perturbing the ith node from the synchronized solution $\mathbf{x}_0(t)$ with amount

$\delta\mathbf{x}_i(t)$, the current state of the ith node becomes $\mathbf{x}_i(t) = \mathbf{x}_0(t) + \delta\mathbf{x}_i(t), i = 1, 2, \ldots, N$. Linearizing each oscillator about the synchronization trajectory $\mathbf{x}_0$, the dynamics of the perturbed system can be written as,

$$\delta\dot{\boldsymbol{x}}_i = Jf(\mathbf{x}_0)\delta\mathbf{x}_i - \sum_{k=1}^{d_{\max}} \epsilon_k \sum_{j=1}^{N} \mathscr{L}_{ij}^{[k]} \Gamma \delta\mathbf{x}_j. \tag{5}$$

Thus the dynamics of the error system in vectorial form yields

$$\delta\dot{\mathbf{x}}(t) = \left[I_N \otimes Jf(\mathbf{x}_0) - \sum_{k=1}^{d_{\max}} \epsilon_k \mathscr{L}^{[k]} \otimes \Gamma \right] \delta\mathbf{x}, \tag{6}$$

where $\delta\mathbf{x}(t)$ is the stack of the vectors $\delta\mathbf{x}_1, \delta\mathbf{x}_2, \ldots, \delta\mathbf{x}_N$, and J is the Jacobian operator, i.e., $Jf(\mathbf{x}_0) = \frac{\partial f(\mathbf{x})}{\partial \mathbf{x}}\big|_{\mathbf{x}=\mathbf{x}_0}$.

The linearized set of equation (6) can be decomposed into two components, one that evolves along the synchronization manifold and the other transverse to it. If the latter components are asymptotically stable, then the set of oscillators (equation (3)) exhibits stable complete synchronization solution. To find the transverse error system, we spectrally decompose $\delta\mathbf{x}(t)$ of the equation (6) and project it onto the basis of the eigenvectors $V^{[1]}$ corresponding to the one-path Laplacian matrix $\mathscr{L}^{[1]}$. Under the Schur transformation onto the space spanned by the basis of eigenvector of $\mathscr{L}^{[1]}$, let $\delta\mathbf{x}(t)$ transforms to $\eta(t) = [\eta_1{}^{\mathrm{tr}}(t), \eta_2{}^{\mathrm{tr}}(t), \ldots, \eta_N{}^{\mathrm{tr}}(t)]^{\mathrm{tr}}$, where $\eta = [V^{[1]} \otimes I_d]^{-1}\delta\mathbf{x}$. Using this Schur transformation, the linearized equation (6) then becomes,

$$\dot{\eta}(t) = \left[I_N \otimes Jf(\mathbf{x}_0) - \sum_{k=1}^{d_{\max}} \epsilon_k \{ V^{[1]^{-1}} \mathscr{L}^{[k]} V^{[1]} \} \otimes \Gamma \right] \eta. \tag{7}$$

Since all the k-path Laplacians $\mathscr{L}^{[k]}$ are real symmetric matrices, so they are orthogonally diagonalizable, and $\mathscr{L}^{[k]} = V^{[k]} D^{[k]} V^{[k]^{-1}}$, where $D^{[k]}$ is the diagonal matrix consisting of the eigenvalues of $\mathscr{L}^{[k]}$ and $V^{[k]}$ is the corresponding matrix of orthogonal eigenvectors. This yields,

$$V^{[1]^{-1}} \mathscr{L}^{[k]} V^{[1]} = V^{[1]^{-1}} V^{[k]} D^{[k]} V^{[k]^{-1}} V^{[1]}. \tag{8}$$

Here each $\mathscr{L}^{[k]}$ is positive semi-definite matrix with at least one zero eigenvalue and the corresponding eigenvector is $\left[\frac{1}{\sqrt{N}}, \frac{1}{\sqrt{N}}, \ldots, \frac{1}{\sqrt{N}}\right]^{\mathrm{tr}}$. Then we consider the form of the matrix $V^{[k]}$ as,

$$V^{[k]} = \begin{bmatrix} \frac{1}{\sqrt{N}} & V_{12}{}^{[k]} & \cdots & V_{1N}{}^{[k]} \\ \frac{1}{\sqrt{N}} & V_{22}{}^{[k]} & \cdots & V_{2N}{}^{[k]} \\ \cdots & \cdots & \cdots & \cdots \\ \frac{1}{\sqrt{N}} & V_{N2}{}^{[k]} & \cdots & V_{NN}{}^{[k]} \end{bmatrix},$$

which is an orthogonal matrix so that ${V^{[k]}}^{-1} = {V^{[k]}}^{\mathrm{tr}}$. Thus we can obtain,

$$ {V^{[1]}}^{-1} V^{[k]} = \begin{bmatrix} 1 & 0 & \cdots & 0 \\ 0 & {V_{22}}^{[1,k]} & \cdots & {V_{2N}}^{[1,k]} \\ \cdots & \cdots & \cdots & \cdots \\ 0 & {V_{N2}}^{[1,k]} & \cdots & {V_{NN}}^{[1,k]} \end{bmatrix}, \quad \text{and} $$

$$ {V^{[k]}}^{-1} V^{[1]} = \begin{bmatrix} 1 & 0 & \cdots & 0 \\ 0 & {V_{22}}^{[k,1]} & \cdots & {V_{2N}}^{[k,1]} \\ \cdots & \cdots & \cdots & \cdots \\ 0 & {V_{N2}}^{[k,1]} & \cdots & {V_{NN}}^{[k,1]} \end{bmatrix}. $$

Without loss of generality, we assume that the first eigenvalue of $\mathscr{L}^{[k]}$ is zero and $D^{[k]} = \mathrm{diag}\left[0, {\gamma_2}^{[k]}, {\gamma_3}^{[k]}, \ldots, {\gamma_N}^{[k]}\right]$. In order to achieve the complete synchronization state, the underlying one-path network should be connected. For disconnected one-path underlying network, emergence of complete synchronization is impossible (detail analytical proof are in the appendix). Thus, $\mathscr{L}^{[1]}$ has exactly one zero eigenvalue, i.e., ${\gamma_1}^{[1]} = 0$ and ${\gamma_i}^{[1]} > 0$ for all $i \geqslant 2$. Henceforth, from equation (8), we have

$$ {V^{[1]}}^{-1} \mathscr{L}^{[k]} V^{[1]} = \begin{bmatrix} 0 & O_{1\times(N-1)} \\ O_{(N-1)\times 1} & U^{[k]} \end{bmatrix}, \tag{9} $$

where $U^{[k]} \in \mathbb{R}^{(N-1)\times(N-1)}$ is a symmetric matrix.

Also we decompose the transformed variable $\eta(t) = [\eta_{\mathrm{P}}(t), \eta_{\mathrm{T}}(t)]$, where $\eta_{\mathrm{P}}(t) \in \mathbb{R}^d$ and $\eta_{\mathrm{T}}(t) \in \mathbb{R}^{(N-1)d}$ are the components parallel and transverse to the synchrony manifold $\mathcal{S}$, respectively. Incorporating this decomposition in equation (7) and with the help of equation (9), the transformed error dynamics becomes,

$$ \begin{aligned} \begin{bmatrix} \dot{\eta}_{\mathrm{P}}(t) \\ \dot{\eta}_{\mathrm{T}}(t) \end{bmatrix} &= \bigoplus_{i=1}^{N} Jf(\mathbf{x}_0) \begin{bmatrix} \eta_{\mathrm{P}}(t) \\ \eta_{\mathrm{T}}(t) \end{bmatrix} - \sum_{k=1}^{d_{\max}} \epsilon_k \begin{bmatrix} 0 & O_{1\times(N-1)} \\ O_{(N-1)\times 1} & U^{[k]} \end{bmatrix} \otimes \Gamma \begin{bmatrix} \eta_{\mathrm{P}}(t) \\ \eta_{\mathrm{T}}(t) \end{bmatrix} \\ &= \begin{bmatrix} Jf(\mathbf{x}_0)\eta_{\mathrm{P}}(t) \\ I_{N-1} \otimes Jf(\mathbf{x}_0)\eta_{\mathrm{T}}(t) \end{bmatrix} - \sum_{k=1}^{d_{\max}} \epsilon_k \begin{bmatrix} O_d & O_{d\times(N-1)d} \\ O_{(N-1)d\times d} & U^{[k]} \otimes \Gamma \end{bmatrix} \begin{bmatrix} \eta_{\mathrm{P}}(t) \\ \eta_{\mathrm{T}}(t) \end{bmatrix}. \end{aligned} \tag{10} $$

Now from the above equation, decomposing the parallel and transverse terms, one can write,

$$ \begin{aligned} \dot{\eta}_{\mathrm{P}}(t) &= Jf(\mathbf{x}_0)\eta_{\mathrm{P}}(t), \\ \dot{\eta}_{\mathrm{T}}(t) &= \left[I_{N-1} \otimes Jf(\mathbf{x}_0) - \sum_{k=1}^{d_{\max}} \epsilon_k U^{[k]} \otimes \Gamma \right] \eta_{\mathrm{T}}(t). \end{aligned} \tag{11} $$

Note that the first equation of equation (11) is the linearized equation of the synchronization solution $\dot{\boldsymbol{x}}_0 = f(\mathbf{x}_0)$. Thus $\eta_{\mathrm{P}}(t)$ corresponds to the projected perturbations within the synchronization manifold, while the second coupled equation is the dynamics of the projected error component transverse to the synchronization manifold. Thus, $\eta_{\mathrm{T}}(t)$ is the transverse error dynamics. Now we make this equation into more simplified form. Since, ${V^{[1]}}^{-1} \mathscr{L}^{[1]} V^{[1]} = D^{[1]}$ and $U^{[1]} = \mathrm{diag}\left\{{\gamma_2}^{[1]}, {\gamma_3}^{[1]}, \ldots, {\gamma_N}^{[1]}\right\}$, then

$$\dot{\eta}_{\mathrm{T}_i}(t) = \left[Jf(\mathbf{x}_0) - \epsilon_1 \gamma_i^{[1]} \Gamma\right] \eta_{\mathrm{T}_i} - \sum_{k=2}^{d_{\max}} \epsilon_k \sum_{j=1}^{N-1} U_{ij}^{[k]} \Gamma \eta_{\mathrm{T}_j}, \quad i = 2, 3, \ldots, N. \tag{12}$$

This completes the proof. □

Remark 1. The eigenspaces of all the k-path Laplacian matrices form N equivalent bases of $\mathbb{R}^N$. Therefore, we are free to choose any one k-path Laplacian eigenspace. Without loss of any generality, here we chose the one-path Laplacian eigenspace.

The above equation (12) is our required transverse master stability equation (MSE) for the complete synchronization solution. It is $(N-1)d$-dimensional coupled equation. In general, the transverse error system (12) cannot be further reduced to low-dimensional form. Also, generally, it is not directly dependent on the eigenvalues of the k-path Laplacians. But, in our case, we can decoupled the MSE (equation (12)) with the help of following corollary.

Corollary 3. *If there exists at least one k-path Laplacian which commutes with all other k-path Laplacians, then the dynamics of the transverse error system can be decoupled as*

$$\dot{\eta}_{\mathrm{T}_i}(t) = \left[Jf(\mathbf{x}_0) - \sum_{k=1}^{d_{\max}} \epsilon_k \gamma_i^{[k]} \Gamma\right] \eta_{\mathrm{T}_i}(t), \quad i = 2, 3, \ldots, N. \tag{13}$$

Proof of corollary 3. Without loss of any generality, we first assume that the one-path Laplacian matrix commutes with all other Laplacian matrices. Additionally, we have the k-path Laplacian matrices for $k = 2, 3, \ldots, d_{\max}$ which are real-symmetric. Therefore, $\mathscr{L}^{[1]}$ and $\mathscr{L}^{[k]}$ share a common eigenspace, for $k = 2, 3, \ldots, d_{\max}$, i.e., they have a common basis of eigenvectors. This yields $V[1] = V^{[k]}$ for $k = 2, 3, \ldots, d_{\max}$.

Thus, $\mathscr{L}^{[k]}$ can be simultaneously diagonalizable by $V^{[1]}$. Then equation (8) expounds

$$V^{[1]^{\mathrm{tr}}} \mathscr{L}^{[k]} V^{[1]} = \mathrm{diag}\left\{\gamma_1^{[k]}, \gamma_2^{[k]}, \ldots, \gamma_N^{[k]}\right\}. \tag{14}$$

This immediately implies that

$$U^{[k]} = \mathrm{diag}\left\{\gamma_2^{[k]}, \gamma_3^{[k]}, \ldots, \gamma_N^{[k]}\right\}. \tag{15}$$

Incorporating the above expression (15), the summation term of equation (12) over j becomes

$$\sum_{j=1}^{N-1} U_{ij}^{[k]} \Gamma \eta_{\mathrm{T}_j} = \gamma_i^{[k]} \Gamma \eta_{\mathrm{T}_i}. \tag{16}$$

Hence, all the coupling terms of the transverse equation (12) become block-diagonal. So, the stability of synchronization is equivalent to the stability of the uncoupled variational equation (13). Thus, the proof is done. □

From the structure of the transverse system, in this way we can able to decouple the effect of coupling term. Here, the Jacobian functions are identical for each block, since they are evaluated on the synchronization state. For each i, the decoupled transverse error systems differ by the scalar multiplier $\epsilon_k \gamma_i^{[k]}$, beyond that the form of the entire equations is same.

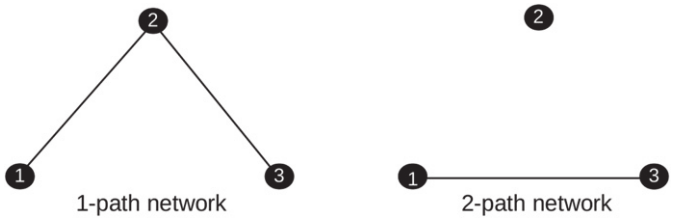

Figure 2. Diagram of the line network with three vertices and corresponding one-path (left panel) and two-path (right panel) networks.

The next remark shows a practical example of such network for which the hypothesis of corollary 3 satisfies.

Remark 2. Consider a line network with number of vertices three. Figure 2 (left panel) depicts the corresponding one-path network. The diameter of this network is 2. The two-path network looks like figure 2 (right panel).

Its two k-path Laplacian matrices are

$$\mathscr{L}^{[1]} = \begin{bmatrix} 1 & -1 & 0 \\ -1 & 2 & -1 \\ 0 & -1 & 1 \end{bmatrix} \quad \text{and} \quad \mathscr{L}^{[2]} = \begin{bmatrix} 1 & 0 & -1 \\ 0 & 0 & 0 \\ -1 & 0 & 1 \end{bmatrix}.$$

It is clear that $\mathscr{L}^{[1]}$ and $\mathscr{L}^{[2]}$ commute with each other. For this network, the transverse error dynamics can be diagonalized according to corollary 3.

Corollary 4. *Let the diameter of the underlying network is two, i.e.,* $d_{\max} = 2$. *Among the two k-path Laplacian matrices, one matrix has eigenvalue 0 with algebraic multiplicity 1 and* $\gamma^{[1]}$ *with algebraic multiplicity* $N-1$. *Then the transverse error dynamics can be decoupled as* $N-1$ *number of d-dimensional systems.*

Proof of corollary 4. Since $d_{\max} = 2$, so there are two k-path Laplacian matrices for $k = 1$ and $k = 2$. Without loss of any generality, let us assume that the one-path Laplacian matrix $\mathscr{L}^{[1]}$ has one eigenvalue 0 with algebraic multiplicity 1 and $\gamma^{[1]}$ with algebraic multiplicity $N-1$. Thus $\gamma_i^{[1]} = \gamma^{[1]}$ for all $i = 2, 3, \ldots, N$.

After decomposing the transformed perturbed variable, the transverse MSE of the complete synchronization solution can be written as

$$\dot{\eta}_{\mathrm{T}_i}(t) = Jf(\mathbf{x}_0)\eta_{\mathrm{T}_i}(t) - \epsilon_1\gamma\Gamma\eta_{\mathrm{T}_i}(t) - \epsilon_2\sum_{j=1}^{N-1} U_{ij}^{[2]}\Gamma\eta_{\mathrm{T}_j}(t). \tag{17}$$

Here, $U^{[2]}$ satisfies $V^{[1]^{-1}}\mathscr{L}^{[2]}V^{[1]} = \begin{bmatrix} 0 & O_{1\times N-1} \\ O_{N-1\times 1} & U^{[2]} \end{bmatrix}$. Also, $\mathscr{L}^{[2]}$ is symmetric matrix, and it can be orthogonally diagonalizable by its basis of eigenvector $V^{[1]}$. Thus, we have $V^{[1]^{-1}} = V^{[1]^{\mathrm{tr}}}$. These results yield

$$\left(V^{[1]^{-1}}\mathscr{L}^{[2]}V^{[1]}\right)^{\mathrm{tr}} = V^{[1]^{\mathrm{tr}}}\mathscr{L}^{[2]}V^{[1]}. \tag{18}$$

So, $\begin{bmatrix} 0 & O_{1\times N-1} \\ O_{N-1\times 1} & U^{[2]} \end{bmatrix}$ is a symmetric matrix and therefore $U^{[2]}$ is also so. Hence, $U^{[2]}$ can be orthogonally diagonalizable by its basis of eigenvectors W (say).

Again, considering a Schur transformation $\xi(t) = [W \otimes I_d]^{-1}\eta_{\Gamma}(t)$, we have the dynamics of the projected error components as,

$$\begin{aligned}\dot{\xi}(t) &= [W \otimes I_d]^{-1}\dot{\eta}_{\Gamma}(t) \\ &= \left[I_{N-1} \otimes Jf(\mathbf{x}_0) - \epsilon_1\gamma I_{N-1} \otimes \Gamma - \epsilon_2 W^{-1}U^{[2]}W \otimes \Gamma\right]\xi(t). \end{aligned} \tag{19}$$

As $W^{-1}U^{[2]}W = \text{diag}\{\gamma_1^{[3]}, \gamma_2^{[3]}, \ldots, \gamma_{N-1}^{[3]}\}$, where $\left\{\gamma_i^{[3]} : i = 1, 2, \ldots, N-1\right\}$ is the set of eigenvalues of $U^{[2]}$. We have our required master stability equation of the transverse error components as,

$$\dot{\xi}_i(t) = \left[Jf(\mathbf{x}_0) - \epsilon_1\gamma\Gamma - \epsilon_2\gamma_i^{[3]}\Gamma\right]\xi_i(t). \tag{20}$$

Which are uncoupled $N-1$ number of d-dimensional systems. □

But, probably this type of networks for which the hypothesis of the above corollary 3 satisfies are very few. Especially for our ER random network with $N = 200$ number of nodes, the k-path Laplacian matrices become non-commutative, for which the transverse error dynamics remains coupled.

We can measure the exponential contraction or expansion of the linearized variational equation by calculating its Lyapunov exponents. Among all the Lyapunov exponents, the maximum one (say Λ) plays a key role. If Λ is less than zero, the complete synchronization state turns out to be locally stable, while its positive value indicates the instability of the synchronization state. By adjusting the tuning parameters (coupling as well as network parameters), we can trace-out the synchronization region where the value of Λ is negative.

5. Emergence of complete synchrony: numerical results

This section is devoted to the discussion of our principal results obtained through numerical simulations. Here, our main emphasis is to verify the above analytical findings. For this, without loss of generalization, we choose the chaotic Lorenz system [40] described as the following:

$$f(\mathbf{x}) = \begin{bmatrix} \sigma(y-x) \\ x(\rho - z) - y \\ xy - \beta z \end{bmatrix}, \tag{21}$$

where $\mathbf{x} = [xyz]^{\text{tr}}$. We fix the system parameters at $\sigma = 10, \rho = 28$ and $\beta = \frac{8}{3}$ for which the system remains in chaotic state. We also choose $\Gamma = \text{diag}[1, 1, 1]^{\text{tr}}$, i.e., coupling through all the three state variables. Here we note that although for the numerical computations, we have chosen Lorenz systems as the local dynamical units, our entire theoretical results have been carried out while considering a general networked system with arbitrary dynamical system over any underlying network topology. The only criteria for our theoretical analysis are that the local dynamics should be continuously differentiable (for local stability analysis) and Lipschitz (for global stability analysis). Hence our analysis remains valid for all the situations in which dynamical systems are interacting through long-range connections.

As mentioned earlier, we here scrutinize the impact of power-law decay of the interaction strength with respect to the distance between the concerned nodes. Specifically, if ϵ_k is the coupling strength between the nodes having shortest distance k ($k = 1, 2, \ldots, d_{\max}$), then $\epsilon_k = \frac{\epsilon}{k^{\alpha}}$

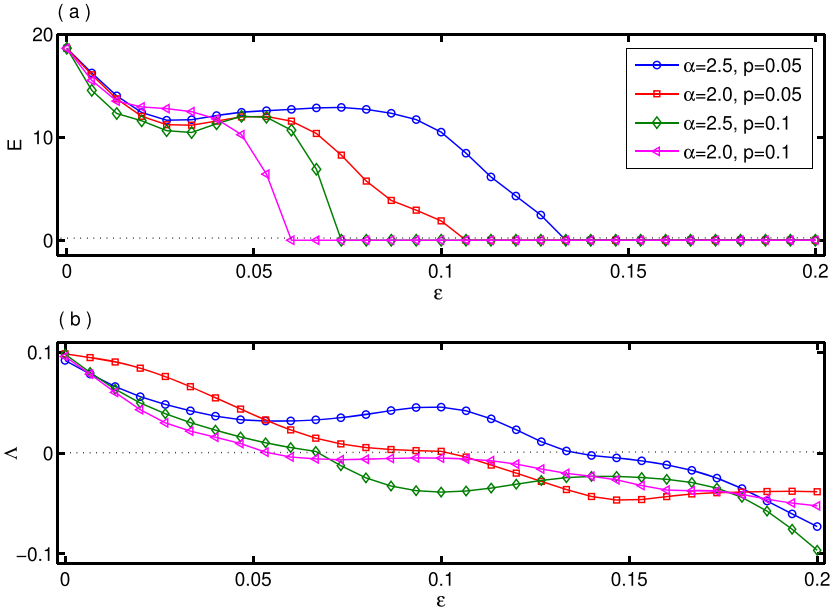

Figure 3. Variation of (a) the synchronization error E and (b) the largest Lyapunov exponent Λ of the transverse error system with respect to the coupling strength ϵ for different combinations of α and p. Here the pairs ($\alpha = 2.5, p = 0.05$), ($\alpha = 2.0, p = 0.05$), ($\alpha = 2.5, p = 0.1$) and ($\alpha = 2.0, p = 0.1$) are chosen and are shown by the blue circle, red square, green diamond, and magenta triangle lines, respectively.

where α is the power-law exponent governing the decay rate. Here we consider the underlying network as the ER random network architecture. Specifically, we choose the $G(N, p)$ graph model [38] with $N = 200$ as the number of nodes and p as the connection probability. To draw all the numerical figures, we have taken ten network realizations at each grid point.

For this type of network, $d_{\max}$ will depend on p. When $p = 1$, each node of the network is directly connected to all the other nodes, as a result of which the value of $d_{\max}$ will also be 1. However, as p decreases $d_{\max}$ will monotonically increase (may not be strictly). Finally, at a certain value of p, $d_{\max}$ will reach its maximum value. Beyond that critical value of p, the underlying network becomes disconnected and $d_{\max}$ is undefined, as the distance between two nodes from two different network components is not defined.

The network of coupled system given in equation (3) together with the isolate dynamics equation (21) is integrated using the Runge–Kutta–Fehlberg method with an integration time step $\Delta t = 0.01$. The time interval for our entire numerical simulations is taken over 1×10^5 iterations after an initial transient of 2×10^5 iterations. The initial conditions for each local dynamical unit are chosen randomly from the phase space in which the chaotic attractor resides. We first define the synchronization error as the following

$$E = \lim_{T\to\infty} \frac{1}{T} \int_t^{t+T} \sum_{i,j=1(i\neq j)}^{N} \frac{\|\mathbf{x}_i(t) - \mathbf{x}_j(t)\|}{N(N-1)} \, \mathrm{d}t. \tag{22}$$

For the numerical simulation we have chosen $t = 2000$ and $T = 1000$. As conspicuous from its definition, in the state of complete synchronization, E necessarily becomes zero, and remains non-zero for the states of desynchrony.

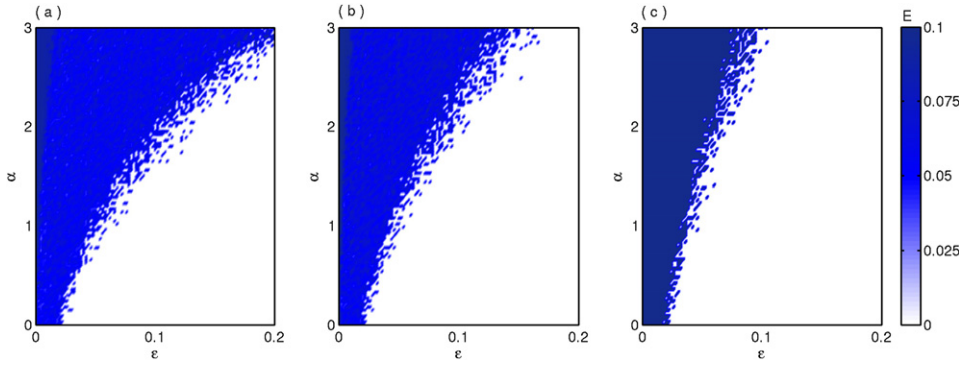

Figure 4. Phase diagram in the (ϵ, α) coupling parameters' plane in terms of the synchronization error E for ER random network with (a) $p = 0.035$, (b) $p = 0.05$, and (c) $p = 0.1$.

First, we initiate our results with looking at the variation in the synchronization error E as a function of the interaction strength ϵ for different values of the power-law exponent α and connection probability p in figure 3(a). The blue curve is plotted for $\alpha = 2.5$ and $p = 0.05$. For $\epsilon = 0.0$, starting with non-zero value, E decreases and eventually drops down to zero for $\epsilon = 0.1333$. Basically this signifies the emergence of complete synchronization in the network for chosen values of α and p. Next, we decrease α to $\alpha = 2.0$ and observe that E (red curve) becomes zero comparatively at lower $\epsilon = 0.1067$. This enhancement of the synchrony occurs due to the lower decaying rate. Then we deal with higher values of $p = 0.1$. For $\alpha = 2.5$, the transition from desynchrony to synchrony occurs at $\epsilon = 0.0733$ (presented in green curve). Actually the increment in p leads to a higher connection probability, i.e., higher link density and hence lower diameter of the network so that lower ϵ is required to achieve complete synchrony. Then we deal with a different value of α, namely $\alpha = 2.0$ by magenta curve. This results in stronger decay in the coupling strength with respect to the shortest distance among the nodes. For this α, we see that even lower ϵ values are sufficient for acquiring synchronization, e.g., E turns into zero near $\epsilon = 0.06$. However, in the error plots strong fluctuations are present due to the randomness in a finite-sized system.

Now, we investigate the stability of synchronization state in terms of the maximum transverse Lyapunov exponent. The existence criterion for synchronization manifold is analytically derived by a linear stability analysis in terms of the MSF approach. We will verify the transition point from desynchronization to synchronization by plotting the transverse Lyapunov exponent. For our network model, we can write the traverse error dynamics equation (12) as

$$\begin{aligned}
\dot{\eta}^{(x)}_{\mathrm{T}_i} &= \sigma(\eta^{(y)}_{\mathrm{T}_i} - \eta^{(x)}_{\mathrm{T}_i}) - \epsilon_1 \gamma^{[1]}_i \eta^{(x)}_{\mathrm{T}_i} - \sum_{k=2}^{d_{\max}} \epsilon_k \sum_{j=1}^{N-1} U^{[k]}_{ij} \eta^{(x)}_{\mathrm{T}_j}, \\
\dot{\eta}^{(y)}_{\mathrm{T}_i} &= (\rho - z_0)\eta^{(x)}_{\mathrm{T}_i} - \eta^{(y)}_{\mathrm{T}_i} - x_0 \eta^{(z)}_{\mathrm{T}_i} - \epsilon_1 \gamma^{[1]}_i \eta^{(y)}_{\mathrm{T}_i} - \sum_{k=2}^{d_{\max}} \epsilon_k \sum_{j=1}^{N-1} U^{[k]}_{ij} \eta^{(y)}_{\mathrm{T}_j}, \\
\dot{\eta}^{(z)}_{\mathrm{T}_i} &= y_0 \eta^{(x)}_{\mathrm{T}_i} + x_0 \eta^{(y)}_{\mathrm{T}_i} - \beta \eta^{(z)}_{\mathrm{T}_i} - \epsilon_1 \gamma^{[1]}_i \eta^{(z)}_{\mathrm{T}_i} - \sum_{k=2}^{d_{\max}} \epsilon_k \sum_{j=1}^{N-1} U^{[k]}_{ij} \eta^{(z)}_{\mathrm{T}_j}, \quad i = 2, 3, \ldots, N.
\end{aligned} \tag{23}$$

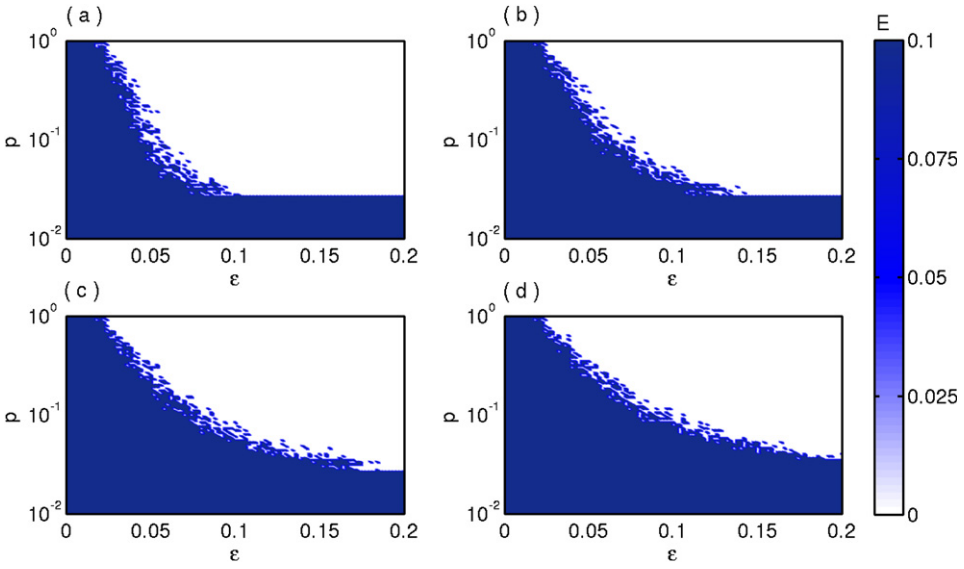

Figure 5. Variation of the synchronization error in the (ϵ, p) parameter space for (a) $\alpha = 1.5$, (b) $\alpha = 2.0$, (c) $\alpha = 2.5$, and (d) $\alpha = 3.0$.

Here (x_0, y_0, z_0) is the state variable of the synchronized manifold whose equation of motion is: $\dot{x}_0 = \sigma(y_0 - x_0), \dot{y}_0 = x_0(\rho - z_0) - y_0, \dot{z}_0 = x_0 y_0 - \beta z_0$. We compute $N - 1$ number of Lyapunov exponents by solving the linearized equation (5) along with the above synchronized manifold equation. The maximum among these Lyapunov exponents (i.e., master stability function Λ) as a function of ϵ, α and p gives the necessary condition for the stability of the synchronous state. By adjusting these tuning parameters so that Λ is less than zero signify the emergence of synchronous trajectory.

In figure 3(b), the transition from desynchrony to synchrony is characterized by the maximum transverse Lyapunov exponent Λ with respect to ϵ. The curves are plotted for the four different values of α and p as of figure 3(a). For these four cases, Λ crosses zero exactly at that point where the synchronization error becomes zero in figure 3(a), which indicates that our analytical local stability condition agrees well with our numerical simulations of the synchronization error plot. However, for a close inspection, there might be slight differences in the critical values due to the initial conditions.

Figure 4 depicts the synchronization error E as a result of simultaneous variation in the coupling strength $\epsilon \in [0, 0.2]$ and the power-law exponent $\alpha \in [0, 3]$, for three exemplary values of p. In figure 4(a), we plot E for an ER random network with low probability $p = 0.035$ of connection among the nodes. As discernible from the figure, an increment in the interaction strength ϵ leads to the emergence of complete synchrony, but this scenario essentially depends upon the value of the exponent α. As long as α is small enough, i.e., when the decay rate of the coupling strength for long-range interaction is small, then synchrony appears for small coupling strength ϵ. But increasing α needs higher ϵ for the network to be in complete synchrony. Therefore, long-range interaction enhances the synchrony compare to the short-range interaction. Detail discussions regarding the comparison of the short-range and long-range interactions are in the appendix. However, synchrony is achieved for each value of

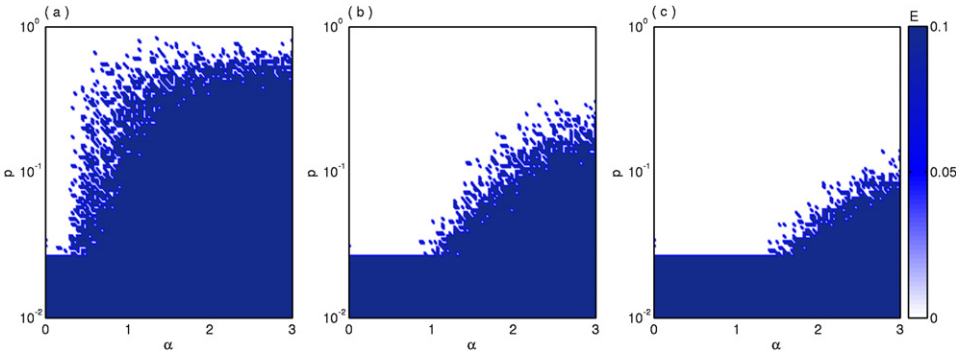

Figure 6. Variation of the synchronization error in the (α, p) parameter space, where the values of ϵ are (a) $\epsilon = 0.03$, (b) $\epsilon = 0.06$, and (c) $\epsilon = 0.09$.

$\alpha \in [0, 3]$ for an appropriate value of ϵ. Next we increase the value of p to $p = 0.05$ and plot E (cf figure 4(b)) in order to portray the similar scenario for higher probability of connection among the nodes. In this case, again higher α demands higher ϵ for synchronization, but the critical transition curve shifts toward left, and helps enlarging the region of synchrony. For a further increment in the value of p to 0.1, similar tendency in the (ϵ, α) parameter plane persists, but for this case the region of synchrony enlarges further as well and the critical curve shifts toward more left.

Now, we investigate the phase diagram in the (ϵ, p) parameter plane, which is depicted in figure 5 in terms of the synchronization error E (color bar) for several values of α. For these four sub-figures, the underlying one-path network becomes disconnected for $p < 0.0263$. For such a network any kind of adjustment of rhythm among the nodes is impossible, that is why the synchronization error E remains non-zero for those p values. The figures 5(a)–(d) are respectively plotted for $\alpha = 1.5$, $\alpha = 2.0$, $\alpha = 2.5$ and $\alpha = 3.0$. For all these four cases, increasing either ϵ or p always leads to the monotonical enhancement of the complete synchronization. On the other hand, as long-range decaying rate α gradually increases, the synchronization region gets shrinked. Here, larger values of the probability p cause gradual decrease in the critical synchrony threshold of ϵ. As we previously observed from figure 3 that the higher values of p yields lower diameter, hence lower coupling strength is required for the emergence of complete synchrony.

In order to reveal the combined effect of the long-range decaying rate α and the network connection probability p on the transition to complete synchrony, we have drawn phase diagrams in the (α, p) plane in figure 6 for three different values of ϵ. Similar to figure 5, no synchrony is observed below $p = 0.0263$ due to the disconnectedness of the network. Here, we observe a significant variation of the synchronization region against change in the tuning parameters α and p. Figures 6(a)–(c) are respectively plotted for $\epsilon = 0.03$, $\epsilon = 0.06$ and $\epsilon = 0.09$. As we gradually increase the value of ϵ, the synchronization region enlarges significantly. For all these three plots, the critical threshold of synchrony in terms of (α, p) enhances by increasing p, but decreasing α. Thus, complete synchronization enhances with respect to the long-range interactions.

In the next section, we devote our study to the investigation of the global stability of the complete synchronization state arising in the network (3). By using Lyapunov function and eigenvalue analysis, we analytically derive the global stability criterion.

6. Global stability analysis

It will strengthen the findings if the condition under which the synchronization solution is globally stable could be derived. For the theory of synchronization, a typical task is to find the condition for its global stability. Before illustrating the main global stability result, we need the following assumptions and lemma based on the dynamics of the isolated node and the topology of the interconnections among the nodes.

Assumption 5. The isolate evolution function $f:\mathbb{R}^d \to \mathbb{R}^d$ satisfies the global Lipschitz condition. So there exists a non-negative constant M such that for any two vectors $\mathbf{x}, \mathbf{y} \in \mathbb{R}^d$,

$$\|f(\mathbf{x}) - f(\mathbf{y})\| \leqslant M \|\mathbf{x} - \mathbf{y}\|. \tag{24}$$

Here, we prove the global stability using Lyapunov-based methods, for which we are assuming the vector-filed of node to be Lipschitz. This assumption gives us an upper bound of the rate of change of the vector field in the phase space.

Assumption 6. The inner coupling matrix Γ is a symmetric positive definite matrix. That is, if $\{\mu_1, \mu_2, \ldots, \mu_d\}$ be the set of eigenvalues of Γ then $\mu_j > 0$ for all $j = 1, 2, \ldots, d$. Moreover, assume that μ_1 is the smallest among the eigenvalues of Γ.

Lemma 7. *The Kronecker product $\left[\mathscr{L}^{[k]} \otimes \Gamma\right]$ of the k-path Laplacian matrix and the inner coupling matrix satisfies the following properties.*

(*a*) *$\left[\mathscr{L}^{[1]} \otimes \Gamma\right]$ has zero eigenvalues with algebraic multiplicity d, and all the other eigenvalues are positive if and only if the one-path network is connected.*
(*b*) *All the eigenvalues of $\left[\mathscr{L}^{[k]} \otimes \Gamma\right]$ are non-negative for all $k = 2, 3, \ldots, d_{\max}$.*
(*c*) *For all $k = 1, 2, \ldots, d_{\max}$, the smallest non-zero eigenvalue of $\left[\mathscr{L}^{[k]} \otimes \Gamma\right]$ satisfies*

$$\lambda_2\left[\mathscr{L}^{[k]} \otimes \Gamma\right] = \min\left\{\frac{e^{\mathrm{tr}}\left[\mathscr{L}^{[k]} \otimes \Gamma\right] e}{e^{\mathrm{tr}} e} : e \in \mathbb{R}^{dN}, \quad e^{\mathrm{tr}} \mathbb{1}_{dN} = 0, \text{ and } e \neq 0\right\}. \tag{25}$$

Proof.

(a) First assume that $\left[\mathscr{L}^{[1]} \otimes \Gamma\right]$ has a zero eigenvalue with algebraic multiplicity d. Now the set of eigenvalues of $\mathscr{L}^{[1]} \otimes \Gamma$ is $\left\{\gamma_i^{[1]}\mu_j : i = 1, 2, \ldots, N \quad \text{and} \quad j = 1, 2, \ldots, d\right\}$.

Since, $\mathscr{L}^{[1]}$ is positive semi-definite and zero-row sum thus $\gamma_1^{[1]} = 0$ and $\gamma_i^{[1]} \geqslant 0$ for $i = 2, 3, \ldots, N$. Thus $\gamma_1^{[1]}\mu_j = 0$ for $j = 1, 2, \ldots, d$. Now as the algebraic multiplicity of the eigenvalue zero of $\mathscr{L}^{[1]} \otimes \Gamma$ is d, therefore $\gamma_i^{[1]}\mu_j > 0$ for all $i = 2, 3, \ldots, N$ and $j = 1, 2, \ldots, d$.

This yields $\gamma_i^{[1]} > 0$ for all $i = 2, 3, \ldots, N$. So the algebraic multiplicity of the eigenvalue zero of $\mathscr{L}^{[1]}$ is one, hence the one-path network is connected.

Conversely, suppose that the one-path network is connected. Then, we may assume $\gamma_1^{[1]} = 0$ and $\gamma_i^{[1]} > 0$ for all $i = 2, 3, \ldots, N$.

Thus, $\gamma_1^{[1]}\mu_j = 0$ for all $j = 1, 2, \ldots, d$ and $\gamma_i^{[1]}\mu_j > 0$ for all $i = 2, 3, \ldots, N$ and $j = 1, 2, \ldots, d$. Therefore, the algebraic multiplicity of the zero eigenvalue of $\mathscr{L}^{[1]} \otimes \Gamma$ is d.

(b) For $k = 2, 3, \ldots, d_{\max}$, the k-path Laplacian $\mathscr{L}^{[k]}$ is by default positive semi-definite. Thus, $\gamma_i^{[k]} \geqslant 0$ for all $i = 1, 2, \ldots, N$. Thus, $\gamma_i^{[1]}\mu_j \geqslant 0$ for all $i = 1, 2, \ldots, N$ and $j = 1, 2, \ldots, d$.

(c) Since, Γ is a symmetric matrix so it is orthogonally diagonalizable. Then there exist an orthogonal matrix Q such that $Q^{\mathrm{tr}}\Gamma Q = \mathrm{diag}\{\mu_1, \mu_2, \ldots, \mu_d\} = D_\Gamma$ (say).

The k-path Laplacian matrix $\mathscr{L}^{[k]}$ is also symmetric positive semi-definite for all $k = 1, 2, \ldots, d_{\max}$. Then, there also exist an orthogonal matrix $V^{[k]}$ such that $V^{[k]^{\mathrm{tr}}}\mathscr{L}^{[k]}V^{[k]} = \mathrm{diag}\{\gamma_1^{[k]}, \gamma_2^{[k]}, \ldots, \gamma_N^{[k]}\} = D^{[k]}$ (say). Without loss of any generality, we assume that the first column of $V^{[k]}$ is $\mathbb{1}_N$.

Now, $\left[V^{[k]} \otimes Q\right]^{\mathrm{tr}} \left[\mathscr{L}^{[k]} \otimes \Gamma\right] \left[V^{[k]} \otimes Q\right] = \left(V^{[k]^{\mathrm{tr}}}\mathscr{L}^{[k]}V^{[k]}\right) \otimes \left(Q^{\mathrm{tr}}\Gamma Q\right) = D^{[k]} \otimes D_\Gamma$. It is a diagonal matrix with non-negative diagonal elements with at least d number of zero diagonal elements.

Consider the matrix $V^{[k]}$ in the form $V^{[k]} = [\mathbb{1}_N\, v_2^{[k]}\, \ldots\, v_N^{[k]}]$. Then for any $e \in \mathbb{R}^{dN}$, we have,

$$\mathrm{e}^{\mathrm{tr}} \left[\mathscr{L}^{[k]} \otimes \Gamma\right] e = \mathrm{e}^{\mathrm{tr}} \left[V^{[k]} \otimes Q\right] \left[D^{[k]} \otimes D_\Gamma\right] \left[V^{[k]} \otimes Q\right]^{\mathrm{tr}} e. \tag{26}$$

If we assume $e = [e_1^{\mathrm{tr}}\, e_2^{\mathrm{tr}}\, \ldots\, e_N^{\mathrm{tr}}]^{tr}$, where $e_i \in \mathbb{R}^d$ for all $i = 1, 2, \ldots, N$, then

$$\mathrm{e}^{\mathrm{tr}} \left[V^{[k]} \otimes Q\right] = \mathrm{e}^{\mathrm{tr}} \left[\mathbb{1}_N\, v_2^{[k]}\, \ldots\, v_N^{[k]}\right] \otimes Q = \left[O_{1\times d}\, \mathrm{e}^{\mathrm{tr}} v_2^{[k]} \otimes Q \ \ldots\ \mathrm{e}^{[k]} v_N^{\mathrm{tr}} \otimes Q\right]. \tag{27}$$

Similarly, we can derive,

$$\left[V^{[k]} \otimes Q\right]^{\mathrm{tr}} e = \begin{bmatrix} O_{d\times 1} \\ v_2^{[k]^{\mathrm{tr}}} \otimes Q^{\mathrm{tr}} e \\ \vdots \\ v_N^{[k]^{\mathrm{tr}}} \otimes Q^{\mathrm{tr}} e \end{bmatrix}. \tag{28}$$

Also, one can write, $D^{[k]} \otimes D_\Gamma = \mathrm{diag}\{O_{d\times d}, \gamma_2^{[k]} D_\Gamma, \ldots, \gamma_N^{[k]} D_\Gamma\}$. Thus with the help of equations (27) and (28), the equation (26) becomes

$$\begin{aligned} \mathrm{e}^{\mathrm{tr}}[\mathscr{L} \otimes \Gamma]e = {} & [O_{1\times d}\, \mathrm{e}^{\mathrm{tr}} v_2^{[k]} \otimes Q \cdots \mathrm{e}^{[k]} v_N^{\mathrm{tr}} \otimes Q] \\ & \times \begin{bmatrix} O_{d\times d} & O_{d\times d} & \cdots & O_{d\times d} \\ O_{d\times d} & \gamma_2^{[k]} D_\Gamma & \cdots & O_{d\times d} \\ \vdots & \vdots & \vdots & \vdots \\ O_{d\times d} & O_{d\times d} & \cdots & \gamma_N^{[k]} D_\Gamma \end{bmatrix} \begin{bmatrix} O_{d\times 1} \\ v_2^{[k]^{\mathrm{tr}}} \otimes Q^{\mathrm{tr}} e \\ \vdots \\ v_N^{[k]^{\mathrm{tr}}} \otimes Q^{\mathrm{tr}} e \end{bmatrix}. \end{aligned} \tag{29}$$

This is equivalent to

$$\mathrm{e}^{\mathrm{tr}}[\mathscr{L} \otimes \Gamma]e = \sum_{i=2}^{N} \gamma_i^{[k]} \mathrm{e}^{\mathrm{tr}} (v_i^{[k]} \otimes Q) D_\Gamma (v_i^{[k]^{\mathrm{tr}}} \otimes Q^{\mathrm{tr}}) e. \tag{30}$$

As $\gamma_2^{[k]} \leqslant \gamma_i^{[k]}$ for all $2 < i$, and μ_1 is smallest among all the eigenvalues of Γ, we then have,

$$\mathrm{e}^{\mathrm{tr}}[\mathscr{L} \otimes \Gamma]e \geqslant \gamma_2^{[k]} \mu_1 \sum_{i=2}^{N} \mathrm{e}^{\mathrm{tr}} (v_i^{[k]} \otimes Q)(v_i^{[k]^{\mathrm{tr}}} \otimes Q^{\mathrm{tr}}) e. \tag{31}$$

Since, $v_1^{[k]} = \mathbb{1}_N$ and $\mathrm{e}^{\mathrm{tr}} \mathbb{1}_{dN} = 0$, therefore

$$\mathrm{e}^{\mathrm{tr}}[\mathscr{L} \otimes \Gamma]e \geqslant \gamma_2^{[k]} \mu_1 \sum_{i=i}^{N} \mathrm{e}^{\mathrm{tr}} (v_i^{[k]} \otimes Q)(v_i^{[k]^{\mathrm{tr}}} \otimes Q^{\mathrm{tr}}) e = \gamma_2^{[k]} \mu_1 \mathrm{e}^{\mathrm{tr}} e. \tag{32}$$

Finally we obtain, the smallest non-zero eigenvalue of $\mathscr{L}^{[k]} \otimes \Gamma$ is $\lambda_2[\mathscr{L}^{[k]} \otimes \Gamma] = \gamma_2^{[k]}\mu_1 \leqslant \frac{e^{tr}[\mathscr{L}\otimes\Gamma]e}{e^{tr}e}$ for all $e \in \mathbb{R}^{dN}$ and $k = 1, 2, \ldots, d_{\max}$.

To prove the expression (25), it is sufficient to show that the above inequality is tight. For this, consider $e = [v_2^{[k]} \otimes v_1^{\Gamma}]$, where $v_2^{[k]}$ is the orthogonal eigenvector of $\mathscr{L}^{[k]}$ corresponding to the eigenvalue $\gamma_2^{[k]}$, and v_1^{Γ} is for Γ corresponding to the eigenvalue μ_1. Then we get,

$$\begin{aligned} e^{tr}[\mathscr{L}^{[k]} \otimes \Gamma]e &= [v_2^{[k]} \otimes v_1^{\Gamma}]^{tr}[\mathscr{L}^{[k]} \otimes \Gamma][v_2^{[k]} \otimes v_1^{\Gamma}] \\ &= (v_2^{[k]^{tr}}\mathscr{L}^{[k]}v_2^{[k]}) \otimes (v_1^{\Gamma^{tr}}\Gamma v_1^{\Gamma}) = \gamma_2^{[k]}\mu_1. \end{aligned}$$

The lemma is then proved. □

The next theorem deals with the global stability condition of the complete synchronization state.

Theorem 8 (Global stability analysis). *Given a connected one-path network of N nodes described by* (3)*. Consider the vector field f of the isolate node is Lipschitz with Lipschitz constant $M > 0$. Then, if the k-path coupling strength ϵ_k satisfies the following condition*

$$\sum_{k=1}^{d_{\max}} \epsilon_k \lambda_2[\mathscr{L}^{[k]} \otimes \Gamma] > M, \tag{33}$$

the complete synchronization state of the dynamical network (3) *will be globally stable.*

Proof. Let us first define a new quantity $\bar{\mathbf{x}} = \frac{1}{N}\sum_{l=1}^{N} \mathbf{x}_l(t)$, and let $e_i = \mathbf{x}_i - \bar{\mathbf{x}}$. Then the dynamics of this average can be written as,

$$\begin{aligned} \dot{\bar{\mathbf{x}}} &= \frac{1}{N}\sum_{l=1}^{N} \dot{\boldsymbol{x}}_l \\ &= \frac{1}{N}\sum_{l=1}^{N} f(\mathbf{x}_l) - \frac{1}{N}\sum_{l=1}^{N}\sum_{k=1}^{d_{\max}} \epsilon_k \sum_{j=1}^{N} \mathscr{L}_{lj}^{[k]}\Gamma\mathbf{x}_j \\ &= \frac{1}{N}\sum_{l=1}^{N} f(\mathbf{x}_l) - \frac{1}{N}\sum_{k=1}^{d_{\max}} \epsilon_k \sum_{j=1}^{N}\sum_{l=1}^{N} \mathscr{L}_{lj}^{[k]}\Gamma\mathbf{x}_j. \end{aligned} \tag{34}$$

But, since each $\mathscr{L}^{[k]}$ is zero-row sum and symmetric, so $\sum_{l=1}^{N} \mathscr{L}_{lj}^{[k]} = 0$ for all $j = 1, 2, \ldots, N$. Thus $\dot{\bar{\mathbf{x}}} = \frac{1}{N}\sum_{l=1}^{N} f(\mathbf{x}_l)$.

Again, $\mathscr{L}^{[1]}$ is the one-path Laplacian matrix or simply the Laplacian matrix of the underlying network, so $\mathscr{L}^{[1]}$ has a simple zero eigenvalue and all the other eigenvalues are positive. Moreover, the k-path Laplacian matrix $\mathscr{L}^{[k]}(k = 2, 3, \ldots, d_{\max})$ is also symmetric and positive semi-definite. But it may have more than one zero eigenvalue. From lemma 7, the second smallest eigenvalue $\lambda_2[\mathscr{L}^{[k]}]$ of $\mathscr{L}^{[k]}(k = 2, 3, \ldots, d_{\max})$ satisfies

$$\lambda_2[\mathscr{L}^{[k]}] = \min_{v^{tr}\mathbb{1}_N = 0, v \neq 0} \frac{v^{tr}\mathscr{L}^{[k]}v}{v^{tr}v}, \tag{35}$$

where $\mathbb{1}_N = [1, 1, \ldots, 1]^{tr}$.

We assume that the vector field of the uncoupled nodes is Lipschitz, i.e., $\|f(\mathbf{x}) - f(\mathbf{y})\| \leqslant M\|\mathbf{x} - \mathbf{y}\|$, where M is the Lipschitz constant.

Let us now consider the Lyapunov function $V = \frac{1}{2}\sum_{i=1}^{N} {e_i}^{\mathrm{tr}} e_i$. Its time derivative along the network dynamics can be written as

$$\dot{V}(t) = \sum_{i=1}^{N} {e_i}^{\mathrm{tr}} \dot{e}_i = \sum_{i=1}^{N} {e_i}^{\mathrm{tr}} [\dot{\mathbf{x}}_i - \dot{\bar{\mathbf{x}}}] = \sum_{i=1}^{N} {e_i}^{\mathrm{tr}} \left[f(\mathbf{x}_i) - \sum_{k=1}^{d_{\max}} \epsilon_k \sum_{j=1}^{N} \mathscr{L}_{ij}^{[k]} \Gamma \mathbf{x}_j - \frac{1}{N} \sum_{l=1}^{N} f(\mathbf{x}_l) \right]. \tag{36}$$

Now, notice that $\sum_{i=1}^{N} {e_i}^{\mathrm{tr}} \left[f(\bar{\mathbf{x}}) - \frac{1}{N}\sum_{l=1}^{N} f(\mathbf{x}_l) \right] = 0$, due to $\sum_{i=1}^{N} e_i = 0$. So, we get $\sum_{i=1}^{N} {e_i}^{\mathrm{tr}} f(\bar{\mathbf{x}}) = \sum_{i=1}^{N} {e_i}^{\mathrm{tr}} \frac{1}{N}\sum_{l=1}^{N} f(\mathbf{x}_l)$. Using this equality, the aforementioned equation (36) becomes

$$\begin{aligned} \dot{V}(t) &= \sum_{i=1}^{N} {e_i}^{\mathrm{tr}} \left[f(\mathbf{x}_i) - \sum_{k=1}^{d_{\max}} \epsilon_k \sum_{j=1}^{N} \mathscr{L}_{ij}^{[k]} \Gamma \mathbf{x}_j - f(\bar{\mathbf{x}}) \right] \\ &= \sum_{i=1}^{N} {e_i}^{\mathrm{tr}} [f(\mathbf{x}_i) - f(\bar{\mathbf{x}})] - \sum_{k=1}^{d_{\max}} \epsilon_k \sum_{i=1}^{N} {e_i}^{\mathrm{tr}} \sum_{j=1}^{N} \mathscr{L}_{ij}^{[k]} \Gamma (\mathbf{x}_j - \bar{\mathbf{x}}). \end{aligned} \tag{37}$$

Recall now that f is a Lipschitz function. This implies that for any two vectors $\mathbf{x}_i$ and $\bar{\mathbf{x}} \in \mathbb{R}^d$, we have

$$\dot{V}(t) \leqslant M \sum_{i=1}^{N} {e_i}^{\mathrm{tr}} (\mathbf{x}_i - \bar{\mathbf{x}}) - \sum_{k=1}^{d_{\max}} \epsilon_k \sum_{i=1}^{N} {e_i}^{\mathrm{tr}} \sum_{j=1}^{N} \mathscr{L}_{ij}^{[k]} \Gamma e_j. \tag{38}$$

If $\mathbf{e}$ denotes the stack of e_i, then in vectorial form the above inequality can be written as

$$\dot{V}(t) \leqslant M \mathbf{e}^{\mathrm{tr}} \mathbf{e} - \sum_{k=1}^{d_{\max}} \epsilon_k \mathbf{e}^{\mathrm{tr}} [\mathscr{L}^{[k]} \otimes \Gamma] \mathbf{e}. \tag{39}$$

Now, $\mathbf{e}^{\mathrm{tr}} \mathbb{1}_N = \sum_{j=1}^{N} e_j = \sum_{j=1}^{N} (\mathbf{x}_j - \bar{\mathbf{x}}) = 0$, thus by lemma 7, we have,

$$\min_{\mathbf{e} \neq 0} [\mathbf{e}^{\mathrm{tr}} (\mathscr{L}^{[k]} \otimes \Gamma) \mathbf{e}] = \lambda_2 [\mathscr{L}^{[k]} \otimes \Gamma] \mathbf{e}^{\mathrm{tr}} \mathbf{e}. \tag{40}$$

Incorporating the expression (40) in the inequality (39), we have

$$\dot{V}(t) \leqslant M \mathbf{e}^{\mathrm{tr}} \mathbf{e} - \sum_{k=1}^{d_{\max}} \epsilon_k \lambda_2 [\mathscr{L}^{[k]} \otimes \Gamma] \mathbf{e}^{\mathrm{tr}} \mathbf{e} = \left[M - \sum_{k=1}^{d_{\max}} \epsilon_k \lambda_2 [\mathscr{L}^{[k]} \otimes \Gamma] \right] \mathbf{e}^{\mathrm{tr}} \mathbf{e}. \tag{41}$$

So the complete synchronization state will be globally stable if $\dot{V}$ is negative definite, i.e., $\left(M - \sum_{k=1}^{d_{\max}} \epsilon_k \lambda_2 [\mathscr{L}^{[k]} \otimes \Gamma] \right) < 0$.

Now since the one-path network is connected, so by lemma 7, at least $\lambda_2 [\mathscr{L}^{[1]} \otimes \Gamma]$ is positive. Thus we obtain suitable coupling strengths ϵ_k, $k = 1, 2, \ldots, d_{\max}$ for which the required condition is satisfied.

This completes the proof. □

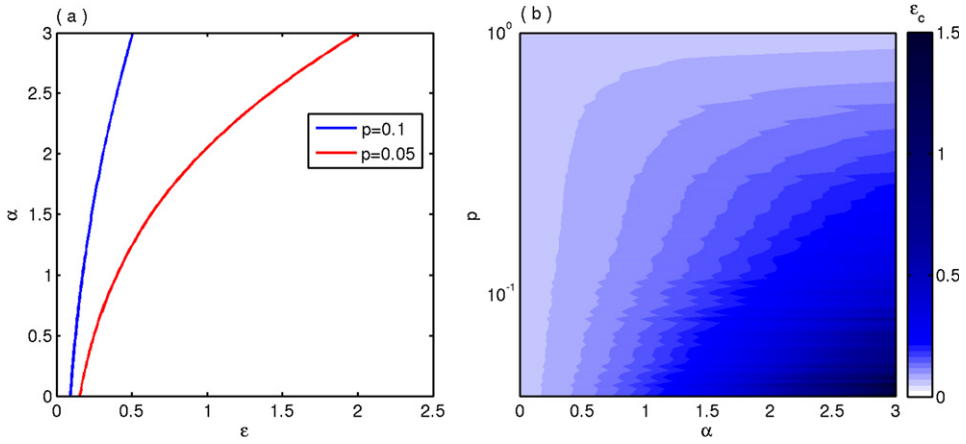

Figure 7. (a) Global stability curve in the (ϵ, α) parameter space for two different values of $p : p = 0.05$ (red line) and $p = 0.1$ (blue line). (b) Variation of the critical coupling strength ϵ_c in the (α, p) parameter plane (from our global stability results).

Above theorem provides a sufficient condition for the global stability of the complete synchronization state in terms of appropriate coupling strength. This global stability result depends directly on the eigenvalues of $L^{[k]}$ for $k = 1, 2, \ldots, d_{\max}$. Below we derive this condition for our coupling architecture.

Remark 3. For power-law decaying rate, the coupling strength for shortest-distance k is $\epsilon_k = \frac{\epsilon}{k^\alpha}$. Then the global stability condition becomes

$$\epsilon > \frac{M}{\sum_{k=1}^{d_{\max}} \frac{\lambda_2[\mathscr{L}^{[k]} \otimes \Gamma]}{k^\alpha}}. \tag{42}$$

Therefore, the global stability condition depends on the Lipschitz constant M, minimum non-zero eigenvalue of $\mathscr{L}^{[k]} \otimes \Gamma$ and the power-law exponent α. From the expression (42), it is clear that as α increases, larger coupling strength is needed for the global stability. Thus by considering long-range interactions, global stability of the synchronization also enhances.

Additionally, we have assumed that the inner coupling matrix Γ to be the identity matrix of order 3. Thus all of its three eigenvalues are 1, so $\lambda_2[\mathscr{L}^{[k]} \otimes \Gamma] = \lambda_2[\mathscr{L}^{[k]}]$. Therefore, the global stability condition of equation (3) is

$$\epsilon > \frac{M}{\sum_{k=1}^{d_{\max}} \frac{\lambda_2[\mathscr{L}^{[k]}]}{k^\alpha}} \tag{43}$$

Beyond this coupling strength, all the oscillators in the network converge toward the identical trajectory, irrespective of the initial conditions. The left-hand side of the inequality (43) is termed as the critical coupling threshold for the global stability, and denoted by ϵ_c. Next we look at the variation of ϵ_c with respect to α and p.

Now, we validate numerically the aforementioned global stability results. The Lipschitz constant of the Lorenz system for the chosen parameter values is $M = 11.5$.

The global stability curves in the (ϵ, α) parameter plane are depicted in figure 7(a) for two different values of p. The red curve is for $p = 0.05$ and the blue is for $p = 0.1$. For each curve, its upper region corresponds to the global stability region of the synchronization state. Both the

two curves illustrate that the critical coupling for the global stability monotonically increases for gradually increasing α. But the critical values decrease for increasing connection probability p. For a better visualization, we have plotted the critical coupling strength ϵ_c in the (α, p) parameter plane in figure 7(b). The color bar represents the variation of ϵ_c, where deep blue color recounts the critical coupling strength is approximately equal to 1.5 and white color for ϵ_c near to zero. This sub-figure illustrates more clearly the monotonic enhancement of ϵ_c with respect to p, and de-enhancement with respect to α. A prominent variation of ϵ_c is delineated here.

Since this critical threshold is based upon the Lyapunov stability criterion, more accurate global stability threshold may be found by assuming more optimal Lyapunov function or by any another method. This numerical illustration also verifies our analytical predictions that the long-range interactions enhances the synchronization.

7. Conclusion

There exists a large volume of results in the literature related to the analysis of the synchronization process in coupled systems, even in coupled systems' networks having diverse complex yet realistic architectures. But, comparatively much lesser attention has been paid to the exploration of this phenomenon in systems undergoing long-range interaction. Long-range interaction is characterized as the one that generalizes the conventional direct communication among the nodes based on one-path Laplacian matrix. Rather, such an interaction incorporates all the possible k-path couplings between all the pairs of nodes expressed in terms of k-path Laplacian matrices. In this work, we have presented our results on the manifestation of complete synchronization in ER random network subject to long-range interactions. In order to describe the impact of long-range couplings, we have chosen the decaying interaction strength among the nodes with reference to the power-law, while considering the paradigmatic Lorenz systems for casting the nodes in the network. We have shown how the appearance of synchrony depends on the variation of the coupling strength and the power-law exponent. More importantly, we have provided comprehensive analysis on the stability of the obtained synchronization solution. Besides a thorough investigation of local stability based on the master stability function approach, we also presented global stability analysis for appropriate choice of Lyapunov function. Note that the local stability results give the exact critical coupling strength only for considerably small perturbations. While the critical coupling strength obtained from the global stability analysis is larger then the local case, but irrespective of the perturbations (whether small or large).

Appendix A

In this appendix, we discuss the results for disconnected one-path Laplacian matrix and also discuss the comparision between short-range and long-range interations for complete synchronization.

A.1. Disconnected one-path Laplacian matrix

In this subsection, we prove that the adjustment of rhythm among the nodes is impossible if the network is disconnected, even if we consider long-range interaction.

Proposition 9. *If the underlying one-path is disconnected, then complete synchronization is impossible to occur in the network of coupled system* (3).

Proof of proposition 9. By hypothesis, underlying one-path network is disconnected. For the time being, assume that the one-path network has g components, each one is connected. Then the corresponding Laplacian matrix becomes reducible, and it can be written as the direct sum of g matrices. Hence, we can write $\mathscr{L}^{[1]}$ as $\mathscr{L}^{[1]} = \oplus_{l=1}^{g} \mathscr{L}^{[1,l]}$, where each $\mathscr{L}^{[1,l]}$ is a zero-row sum positive definite matrix. Actually they are the Laplacian matrices of the g disjoint components.

Also assume that the lth component has n_l number of nodes for $l = 1, 2, \ldots, g$ and $\sum_{l=1}^{g} n_l = N$.

Now it is clear that all the k-path networks will have at least g components for $k = 2, 3, \ldots, d_{\max}$. Therefore, this k-path Laplacian can also be written as $\mathscr{L}^{[k]} = \oplus_{l=1}^{g} \mathscr{L}^{[k,l]}$.

While $\mathscr{L}^{[k,l]}$ is also zero-row sum positive semi-definite matrix, but it may be again reducible. In other words, the k-path network may have more than g components. Consequently the algebraic multiplicity of the zero eigenvalue in $\mathscr{L}^{[k]}$ may be greater than g for some $k = 2, 3, \ldots, d_{\max}$.

For each $\mathscr{L}^{[k,l]}$, we can get an orthogonal matrix $V^{[k,l]}$ such that $\mathscr{L}^{[k,l]^{-1}} \mathscr{L}^{[k,l]} V^{[k,l]}$ is a diagonal matrix. This yields,

$$\begin{aligned}\left(\bigoplus_{l=1}^{g} V^{[k,l]}\right)^{-1} \mathscr{L}^{[k]} \left(\bigoplus_{l=1}^{g} V^{[k,l]}\right) &= \bigoplus_{l=1}^{g} \left(V^{[k,l]^{-1}} \mathscr{L}^{[k,l]} V^{[k,l]}\right) \\ &= \operatorname{diag}\left\{\gamma_1^{[k]}, \gamma_2^{[k]}, \ldots, \gamma_N^{[k]}\right\}.\end{aligned} \tag{44}$$

So, $\oplus_{l=1}^{g} V^{[k,l]}$ becomes the orthogonal basis of eigenvectors of $\mathscr{L}^{[k]}$. Which splits the error components into transverse and parallel directions.

Proceeding with the same argument as of equation (9), one can get

$$V^{[1,l]^{-1}} \mathscr{L}^{[k,l]} V^{[1,l]} = \begin{bmatrix} 0 & O_{1\times n_l - 1} \\ O_{n_l - 1 \times 1} & U^{[k,l]} \end{bmatrix}, \tag{45}$$

for all $l = 1, 2, \ldots, g$, where $U^{[k,l]} \in \mathbb{R}^{n_l - 1 \times n_l - 1}$. Right away we can get

$$V^{[1]^{-1}} \mathscr{L}^{[k]} V^{[1]} = \bigoplus_{l=1}^{g} \begin{bmatrix} 0 & O_{1\times n_l - 1} \\ O_{n_l - 1 \times 1} & U^{[k,l]} \end{bmatrix}. \tag{46}$$

With the help of the above matrix equation, we can write the entire variational equation as

$$\begin{bmatrix} \dot{\eta}_{\mathrm{P}}(t) \\ \dot{\eta}_{\mathrm{T}}(t) \end{bmatrix} = \bigoplus_{l=1}^{N} Jf(\mathbf{x}_0) \begin{bmatrix} \eta_{\mathrm{P}}(t) \\ \eta_{\mathrm{T}}(t) \end{bmatrix} - \sum_{k=1}^{d_{\max}} \epsilon_k \bigoplus_{l=1}^{g} \begin{bmatrix} 0 & O_{1\times n_l - 1} \\ O_{n_l - 1 \times 1} & U^{[k,l]} \end{bmatrix} \otimes \Gamma \begin{bmatrix} \eta_{\mathrm{P}}(t) \\ \eta_{\mathrm{T}}(t) \end{bmatrix}. \tag{47}$$

From the above equation eliminating one d-dimensional parallel component, the transverse error dynamics can be written as

$$\dot{\eta}_{\mathrm{T}}(t) = \left\{ \bigoplus_{l=1}^{N-1} Jf(\mathbf{x}_0) - \sum_{k=1}^{d_{\max}} \epsilon_k U^{[k,1]} \bigoplus \bigoplus_{l=2}^{g} \begin{bmatrix} 0 & O_{1\times n_l - 1} \\ O_{n_l - 1 \times 1} & U^{[k,l]} \end{bmatrix} \otimes \Gamma \right\} \eta_{\mathrm{T}}(t). \tag{48}$$

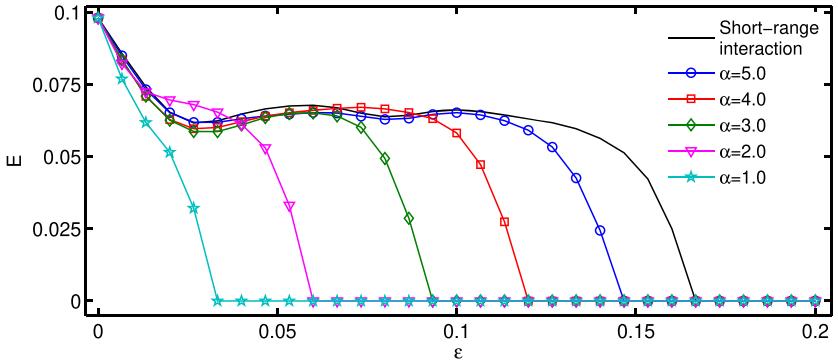

Figure A1. Variation of the synchronization error E with respect to ϵ by considering short-range interactions (black curve) and long-range interactions with different values of power-law exponent $\alpha = 5.0$ (blue circle curve), $\alpha = 4.0$ (red square curve), $\alpha = 3.0$ (green diamond curve), $\alpha = 2.0$ (magenta triangle curve) and $\alpha = 1.0$ (cyan star curve). Other parameter: $p = 0.1$.

If we consider $\eta_{\mathrm{T}}(t)$ is the stack of g vectors $\zeta_1(t), \zeta_2(t), \ldots, \zeta_N(t)$, corresponding to each component, then the above equation is equivalent to g equations as follows,

$$\dot{\zeta}_1(t) = \left\{ \bigoplus_{l=1}^{n_1-1} Jf(\mathbf{x}_0) - \sum_{k=1}^{d_{\max}} \epsilon_k U^{[k,1]} \otimes \Gamma \right\} \zeta_1(t), \tag{49a}$$

$$\dot{\zeta}_l(t) = \left\{ \bigoplus_{i=1}^{n_l} Jf(\mathbf{x}_0) - \sum_{k=1}^{d_{\max}} \epsilon_k \begin{bmatrix} 0 & O_{1\times n_l-1} \\ O_{n_l-1\times 1} & U^{[k,l]} \end{bmatrix} \otimes \Gamma \right\} \zeta_l(t), \quad l=2,3,\ldots,g. \tag{49b}$$

The above two equations governs the entire transverse subspace. But equation (49b) yields at least $(g-1)$ number of d-dimensional equations whose equation of motion are $\dot{\eta}_{\mathrm{T}_i} = Jf(\mathbf{x}_0)\eta_{\mathrm{T}_i}$, which will definitely not get stabilized whatever the coupling strength is.

Hence we get our required result. □

A.2. Comparison between short-range and long-range interactions

Here we briefly compare the emergence of synchronization among short-range and long-range interactions. Short-range interaction can only leads to the direct communications among the nodes, while the long-range interactions enable the nodes to interact with other nodes through all possible paths of different lengths.

Figure A1 depicts the synchronization error E as a function of coupling strength ϵ, where the ER network probability is fixed at $p = 0.1$. Blue curve represents by considering only short-range interactions among the coupled oscillators. For this case the complete synchronization emerges at $\epsilon \simeq 0.1667$. By considering also the long-range interactions, this critical coupling strength enhances depending on the power-law exponent α. The blue circle, red square, green diamond, magenta triangle and cyan star curves are respectively for $\alpha = 5.0, 4.0, 3.0, 2.0$, and 1.0, for which the respective critical coupling strengths are $\epsilon = 0.1467, 0.12, 0.0933, 0.06$, and 0.0333. In the limiting case $\alpha = 0$, we have checked that the critical coupling strength enhances to $\epsilon = 0.0267$. A significant enhancement of synchrony can be observed for long-range connections. The results say that lesser the value of α higher the enhancement in the

emergence of synchrony. Finally, if one considers $\alpha = 0$, then the network becomes globally connected and hence the enhancement of synchrony will be maximum. In this context, it is to be noted that the short-range interaction also a limiting case of long-range interaction for which $\alpha \to \infty$.

ORCID iDs

Dibakar Ghosh https://orcid.org/0000-0003-4832-5210

References

[1] Arenas A, Díaz-Guilera A, Kurths J, Moreno Y and Zhou C 2008 *Phys. Rep.* **469** 93
[2] Pikovsky A, Rosenblum M and Kurths J 2003 *Synchronization: A Universal Concept in Nonlinear Science* (Cambridge: Cambridge University Press)
[3] Boccaletti S, Kurths J, Osipov G, Valladares D L and Zhou C S 2002 *Phys. Rep.* **366** 1
[4] Chavez M, Hwang D-U, Amann A, Hentschel H G E and Boccaletti S 2005 *Phys. Rev. Lett.* **94** 218701
[5] Zhou C, Motter A E and Kurths J 2006 *Phys. Rev. Lett.* **96** 034101
[6] Kohar V, Ji P, Choudhary A, Sinha S and Kurths J 2014 *Phys. Rev.* E **90** 022812
[7] Frasca M, Buscarino A, Rizzo A, Fortuna L and Boccaletti S 2008 *Phys. Rev. Lett.* **100** 044102
[8] Gambuzza L V, Frasca M and Gómez-Gardeñes J 2015 *Europhys. Lett.* **110** 20010
[9] Jalan S and Singh A 2016 *Europhys. Lett.* **113** 30002
[10] Rakshit S, Majhi S, Bera B K, Sinha S and Ghosh D 2017 *Phys. Rev.* E **96** 062308
[11] Majhi S, Ghosh D and Kurths J 2019 *Phys. Rev.* E **99** 012308
[12] Rakshit S, Bera B K and Ghosh D 2018 *Phys. Rev.* E **98** 032305
[13] Campa A, Dauxois T and Ruffo S 2009 *Phys. Rep.* **480** 57
[14] Bouchet F, Gupta S and Mukamel D 2010 *Physica* A **389** 4389
[15] Gupta S and Ruffo S 2017 *Int. J. Mod. Phys.* A **32** 1741018
[16] Gupta S and Mukamel D 2010 *Phys. Rev. Lett.* **105** 040602
[17] Joyce M, Morand J, Sicard F and Viot P 2014 *Phys. Rev. Lett.* **112** 070602
[18] Gupta S and Mukamel D 2010 *J. Stat. Mech.* P08026
[19] Teles T N, Gupta S, Cintio P D and Casetti L 2015 *Phys. Rev.* E **92** 020101
[20] Bountis T 2016 *Eur. Phys. J. Spec. Top.* **225** 1017
[21] Raghavachari S and Glazier J A 1995 *Phys. Rev. Lett.* **74** 3297
[22] Cannas S A and Tamarit F A 1996 *Phys. Rev.* B **54** R12661
[23] Uchida N and Golestanian R 2011 *Phys. Rev. Lett.* **106** 058104
[24] Golestanian R, Yeomans J M and Uchida N 2011 *Soft Matter* **7** 3074
[25] Álvarez G A, Suter D and Kaiser R 2015 *Science* **349** 846
[26] Saffman M, Walker T G and Mølmer K 2010 *Rev. Mod. Phys.* **82** 2313
[27] Levin Y, Pakter R and Teles T N 2008 *Phys. Rev. Lett.* **100** 040604
[28] Maródi M, d'Ovidio F and Vicsek T 2002 *Phys. Rev.* E **66** 011109
[29] Anteneodo C, Pinto S E d S, Batista A M and Viana R L 2003 *Phys. Rev.* E **68** 045202
[30] Kuo H-Y and Wu K-A 2015 *Phys. Rev.* E **92** 062918
[31] Chowdhury D and Cross M C 2010 *Phys. Rev.* E **82** 016205
[32] Banerjee T, Dutta P S, Zakharova A and Schöll E 2016 *Phys. Rev.* E **94** 032206
[33] Gupta A, Banerjee T and Dutta P S 2017 *Phys. Rev.* E **96** 042202
[34] Estrada E, Gambuzza L V and Frasca M 2018 *SIAM J. Appl. Dyn. Syst.* **17** 672
[35] Estrada E, Gambuzza L V and Frasca M 2018 *Proc. IEEE Int. Symp. on Circuits and Systems* (*ISCAS*) (IEEE) pp 1–4
[36] Sathiyadevi K, Chandrasekar V K, Senthilkumar D V and Lakshmanan M 2019 *J. Phys. A: Math. Theor.* **52** 184001
[37] Pecora L M and Carroll T L 1998 *Phys. Rev. Lett.* **80** 2109–12
[38] Erdös P and Rényi A 1959 *Publ. Math. Debrecen* **6** 290
[39] Erdös P and Rényi A 1960 *Publ. Math. Inst. Hung. Acad. Sci.* **5** 17
[40] Lorenz E N 1963 *J. Atmos. Sci.* **20** 130